Nanoscale chemical heterogeneity in aromatic polyamide membranes for reverse osmosis applications

Catriona M. McGilvery[a]*, Patricia Abellan[b], Michał M. Kłosowski[a], Andrew G. Livingston[c], João T. Cabral[c], Quentin M. Ramasse[b,d] and Alexandra E. Porter[a]*

[a] Department of Materials and London Centre for Nanotechnology, Imperial College London, SW7 2AZ, UK

[b] SuperSTEM Laboratory, SciTech Daresbury Campus, Daresbury, WA4 4AD

[c] Department of Chemical Engineering, Imperial College London, SW7 2AZ, UK

[d] School of Chemical and Process Engineering & School of Physics and Astronomy, University of Leeds, Leeds LS2 9JT, UK

ABSTRACT

Reverse osmosis membranes are used within the oil and gas industry for sea water desalination on off-shore oilrigs. The membranes consist of three layers of material – a polyester backing layer, a polysulfone support and a polyamide (PA) thin film separating layer. It is generally thought that the PA layer controls ion selectivity within the membrane, but little is understood about its structure or chemistry at the molecular scale. This active polyamide layer is synthesized by interfacial polymerisation at an organic/aqueous interface between *m*-phenylenediamine (MPD) and trimesoyl chloride (TMC), producing a highly cross-linked polyamide (PA) polymer. It has been speculated that the distribution of functional chemistry within this layer could play a role in solute filtration. The only technique potentially capable of probing the distribution of functional chemistry within the active PA layer with sufficient spatial and energy resolution is scanning transmission electron microscopy combined with electron energy-loss spectroscopy (STEM-EELS). Its use is a challenge because organic materials suffer beam-induced damage at relatively modest electron doses. Here we show that it is possible to use the N K-edge to map the active layer of a PA film using monochromated EELS spectrum imaging. The active PA layer is 12 nm thick, which supports previous neutron reflectivity data. Clear changes in the fine structure of the C K-edge across the PA films are measured and we use machine learning to assign fine structure at this edge. Using this method, we map highly heterogeneous intensity variations in functional chemistry attributed to N-C=C bonds within the PA. Similarities are found with previous molecular dynamics simulations of PA showing regions with a higher density of amide bonding as a result of the aggregation process at similar length scales. The chemical pathways that can be deduced may offer a clearer understanding of the transport mechanisms through the membrane.

INTRODUCTION

Polymer membranes have been used for many years in water separation technologies, such as for the provision of clean drinking water and water desalination for industrial processes. Because of the cost of installing desalination plants at sea, much research is being done to improve their performance, particularly by reducing installation weight, to reduce the inherent costs. The performance of membranes for desalination has greatly improved over the last decade, but it continues to be a challenge to enhance performance and reduce energy consumption. Understanding of the structure and chemistry of the polyamide separating layer in reverse osmosis (RO) membranes at the nanometer length scale may enable the design of novel membranes with superior water desalination performance.

Thin film composite (TFC) reverse osmosis membranes used for water separation are composed of a "tight" polyamide (PA) separation layer, sitting on top of more "open" porous ultrafiltration support (typically polysulfone). The polysulfone (PSf) layer is in turn attached to a porous polyester (PET) fabric backing layer, which provides mechanical stability to the membrane, and has a high porosity to allow solutes to pass through.[1] TFC membranes generally have inhomogeneous variations in their structure, chemistry and porosity at micrometer to nanometer scales.[2,3] Commercial polyamide RO membranes have a highly crumpled structure, made up of folds of 10 nm thick PA film, which form the active separating layer.[4] These folds increase the effective surface area of the membranes by approximately 2-4x, and so improve their permeance.[4] The active separating layer acts as a molecular sieve or ion barrier and plays a critical role in water/ion separation. The internal structure of this layer is made up of nanometer scale porosity or modulations in the density of the cross-linked polyamide that play a role in water solvation within the PA.[4,5]

The active PA layer of reverse osmosis membranes is synthesized by an interfacial polymerisation (IP) reaction at the organic/aqueous interface between *m*-phenylenediamine (MPD) and trimesoyl chloride (TMC) (Figure 1a) producing a highly cross-linked polyaromatic PA polymer (Figure 1b). Simulation and experiments suggest that separating layer formation by IP proceeds *via* a mechanism of cluster formation, aggregation and then percolation, resulting in a heterogeneous film nanostructure, with a pore size distribution[2,6,7]. Membranes can be rationalized in terms of coalesced clusters, which can thus exhibit density modulations, and 'aggregate' and 'network'

pores, whose distribution likely impacts the complex water and ion transport processes. The distribution of functional chemistry within the layer may play a role in solute filtration.[5,8-10]

Recently, very flat 10 nm thick PA thin films have been synthesized by an interfacial polymerisation reaction using Cd nanowires, as a template for the PA interfacial polymerization process.[11] These flat films should now make it possible to characterize the role of chemistry, rather than fold-structure, on membrane permanence. By deuterating and hydrogenating the MPD, and employing water and heavy water hydration, we have shown, using neutron reflectivity, that the thin films are ~12 nm thick and the chemical composition and density along the cross-section (xz) of the ultrathin PA films, in both dry and hydrated state, is in fact very homogenous.[5] (Figure 1e). Specular neutron reflectivity (NR) offers exceptional spatial accuracy along the cross-section of the film (z-direction), limited by its surface roughness (~1 nm), but effectively *averages* across the xy plane of the sample (over ~cm^2). As a result, while the NR data show that, on (xy) average, there is no surface enrichment of components or density modulations across the z-direction of the film, it offers limited insight into the possible chemical heterogeneity within the film. Indeed, few techniques have sufficient spatial and energy resolution for probing spatial variations in functional chemistry within the active PA layer. Chemical analysis of organics is mostly limited to micrometer scale techniques, such as Fourier transform infrared spectroscopy (FTIR), or Raman spectroscopy, but these techniques are restricted by their spatial resolution. Although neutron scattering has sufficient z- resolution to map chemistry across the membranes, it does not have the xy resolution required to map nanoscale variations in chemistry of the thin films. An alternative is to use spatially resolved synchrotron-based scanning transmission X-ray microscopy (STXM) for nanoscale chemical mapping.[12] STXM uses incident X-rays focused onto a sample to map functional chemistry within the PA films at the 20 nm length scale. X-ray absorption near-edge structure (XANES) spectra can be collected in the STXM with a spectral resolution of 0.1 eV.[13] Mitchell *et al.*[12] used STXM x-ray absorption spectroscopy (XAS) to study cross sections through the commercially available FT30 reverse osmosis membrane. They identified two polyamide phases on top of the polysulfone support layer with different chemical compositions. Fine structure in the C K ionization edge was resolved and specific chemical bonds could be assigned to each peak in the spectrum. However, the fundamental detection limit for X-rays means STXM-XAS studies are in practice limited to resolutions of around 20 nm and cannot be used to resolve nm scale structural features within the RO membranes. There is also a lack of understanding around the

severity of specimen damage during image acquisition in STXM (discussed for instance by Goode et al.[14]).

The only technique with adequate spatial resolution to map functional chemistry across PA films is scanning transmission electron microscopy combined with electron energy-loss spectroscopy (STEM-EELS). STEM-EELS provides a higher spatial resolution (< 1 nm) than STXM and permits chemical fingerprinting of functional chemistry using core-loss ionization transitions characteristic of the N, C and O constituent elements. Recent advances in electron monochromators[15] now offer the possibility to acquire spatially-resolved EELS in the STEM with an energy resolution that matches, or improves on, the resolution that can be obtained using synchrotron-based X-ray absorption spectroscopy.[16] Achieving sufficient contrast between functional chemistry, combined with the electron beam sensitivity of the PA, presents challenges for the analysis of the PA by EELS spectrum imaging (SI). Principally this is since the inelastic interaction cross section, although comparatively high for organics due to their low Z number, still requires a significant electron dose to create an interpretable signal. Dong et al.[17] acquired EELS chemical maps at the oxygen K edge of a number of polymer blend materials. However the spatial resolution was of the order of tens of nanometers which is insufficient to map nanoscale permeation pathways in RO membranes. Traditionally, imaging and analysis of polymers by TEM has been dose-limited. A number of beam damage studies have been carried out to understand how electron beam damage alters the functional chemistry of polymeric materials[18,19] mostly in image-coupled mode, using either a bright field or diffracted beam, rather than in STEM mode.[20] Electron energy-loss studies to date typically focus on acquiring core-loss EEL spectra from soft materials under dose conditions for which: (i) spectral fine structure is directly observed as a measurable "intensity above background"; and (ii) for which fine structure can be assigned in EELS spectra.[18] A characteristic dose (characteristic electron fluence, D_e) is typically provided for which the specific signal of interest falls below 1/e of an initial intensity value.[20] Due to the obvious correlation in STEM mode between probe size and electron fluence, the spatial resolution for STEM-based EEL spectroscopy in beam sensitive materials is limited by electron dose and it is not always possible to resolve spectral features of beam sensitive samples with high spatial resolution. Here, we explore the possibility of acquiring spatially resolved maps with a resolution of <10 nm across PA membranes, at an electron dose which, while still damaging to the membranes and diminishing the signals arising from functional chemistry within the material even "below the

5

spectral background", still provides valuable (and otherwise unobtainable) information about the local functional chemistry. We show that even under these conditions, the position of peaks (when resolvable) and of relative integrated intensity maxima, correspond well to characteristic PA electron energy loss fine structure known from 'control' undamaged experiments, and is consistent with the chemical content of the sample, suggesting that functional chemistry information can be extracted.
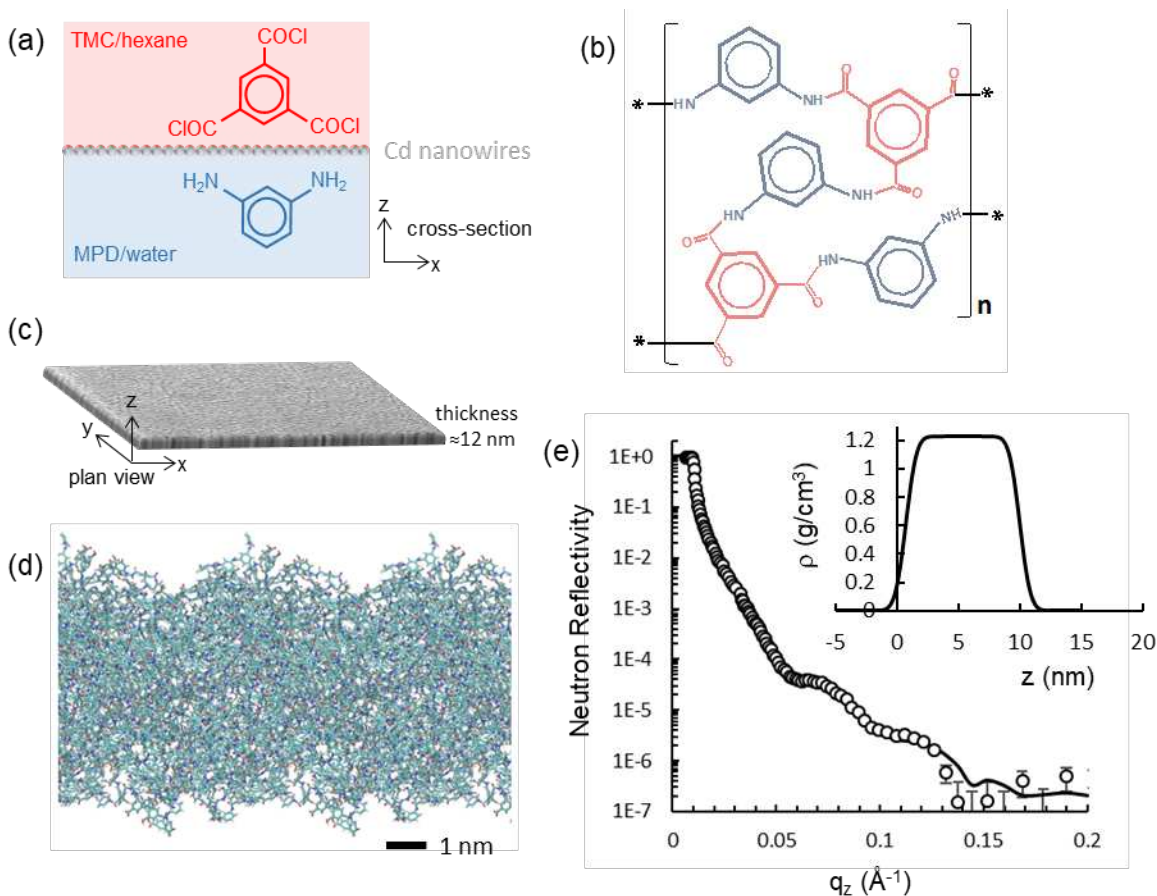
Figure 1 (a) Schematic of the interfacial polymerization of TMC/MPD at the hexane/water interface supported by Cd nanowires[11]. (b) Illustration of a polyamide network with 2 TMC: 3 MPD stoichiometry. (c) Coordinate definition for the microscopy measurement reported here, namely xz cross-sectional view and xy plan view. (d) Molecular dynamics simulation of the PA network, adapted from Ref. 21. (e) Neutron reflectivity measurements establishing a uniform cross-sectional profile (xz) averaged over a large xy area (~cm^2), with a film thickness of approximately 12 nm, and interfacial roughness of ~ 1 nm, adapted from Ref. 5.

RESULTS and DISCUSSION

1. Identification of the EELS spectral fingerprints of functional groups in PA thin films under dose-managed conditions

The 10 nm PA films were analyzed in two different orientations: plan-view and cross-section. In plan-view, EEL spectra from the films at the carbon and the nitrogen ionization K-edges correspond to spatial averages through the thickness of the material and can thus be used as a reference for subsequent EEL spectrum images (SI) taken across cross-sections of the RO membranes. Since in plan-view geometry spatial resolution is not required, damage to the functional chemistry can be reduced by spreading the electron dose used to record the EEL spectra. Here, a typical dose of 1.6-9.6 x 10^3 e/Å^2 per pixel was achieved in plan-view compared with 3.7 x 10^5 e/Å^2 per pixel for the cross sectional data discussed (e.g. in Figure 4). As detailed in the methods section and in the discussion of the influence of acquisition parameters on beam damage, for comparison purposes the probe size was kept the same as for the spatially resolved experiments in cross-section. However, the spectrum images were acquired from a relatively large 800 nm x 800 nm area of the sample, with short dwell times on well-spaced (extremely under-sampled) pixels to produce averaged spectra where electron dose has been minimized (the plan-view spectra presented in Figure 2 were obtained using these conditions). Therefore, EEL spectra taken in this geometry can provide a reference of the fine structure expected to arise from the various functional groups present in the PA film; these can then be compared with spatially resolved maps from cross-section samples. In particular, the clear appearance of peaks and spectral bands in these spectra help with selecting energy windows for signal integration in spectrum images of *cross-sectional* samples, to reveal information about the localization of the corresponding functional groups giving rise to these peaks. We note that differences in thickness between the free-standing plan view samples (about 10 nm thick) and the cross-section samples (about 70 nm thick) mean that the comparison is not perfect due to changes in the interaction volume (so that in effect, more of the inelastic mean free path is being sampled by the electrons travelling through the sample). However previous work reported by Egerton[22] indicates that the thicker the specimen the higher the critical dose. For this reason, it is not expected that data taken from the thicker, cross-section specimens

will cause a loss in fine structure compared to a plan view observation of the same material, all else being equal
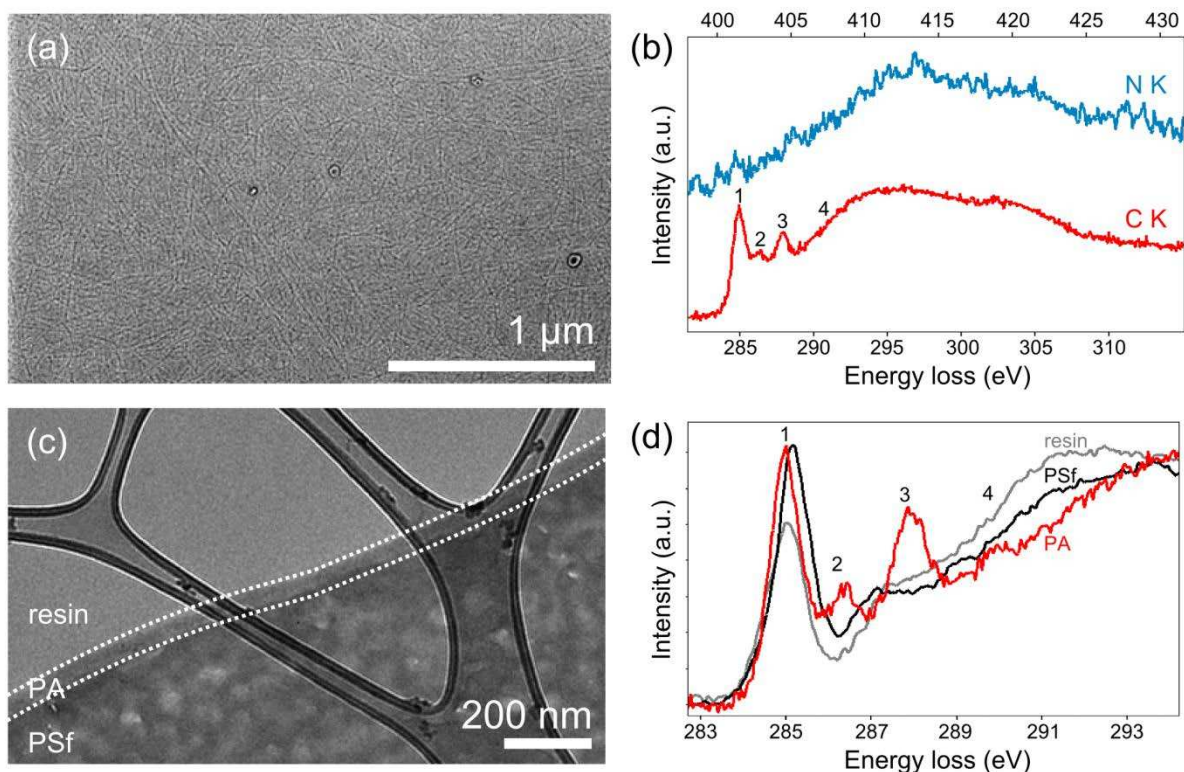

Figure 2 (a) Bright-field TEM image showing the structure of the membrane in plan-view. The image has been taken out of focus to show the underlying criss-cross pattern resulting from the preparation process; (b) C K and N EELS K-edges taken from the plan view sample under dose-managed conditions. The spectra were averaged from an 800 nm x 800 nm area, using a dwell time of 0.02 s/pixel, dispersion of 0.05 eV/pixel (pix) and a pixel spacing of 5.3 nm. (c) BF image of cross-section of an interface between the resin-PA and PSf support. The underlying holey-carbon support film is visible. (d) Comparison of the C K-edge fine structure of the PA, PSf and resin. The PSf and resin spectra were acquired from the cross-section geometry depicted in c, while the PA spectrum is the same as shown in b, overlaid here to demonstrate the clear differentiation between the three components of the samples. All spectra in this figure were taken under the following conditions: 0.02 s/pixel, 0.05 eV/pixel with a pixel spacing of 5.3 nm. This corresponds to an electron fluence of 1.59×10^3 e/Å^2 per pixel size or 7.03×10^6 e/Å^2 per probe size. Peaks 1 – 4 can be assigned to 1s→π*transitions in sp^2-like carbon species and a 1s→σ* peak assigned to 1s-σ* transitions from C-C bonding. These peaks have been assigned as: (1) 1s→π*(C=C$_{aromatic}$), (2) 1s→π*(N-C=C/C=C$_{aromatic}$), (3) 1s→π*(C=O$_{carbonyl}$), (4) 1s→σ*(C=O$_{carbonyl}$) using STXM data.[12]

Plan view. Figure 2a shows a defocused bright field (BF) image of the plan view PA membrane. The imprint of the nanowires used during preparation can be seen on the back side of the membrane. For the EEL spectra in Figure 2b and d, a perfect calibration of the energy dispersion of the spectrometer is challenging to achieve: as a result, the energies of the edges we report here may not be exactly comparable to similar data obtained on other instruments or using STXM-XAS. a direct comparison of relative shifts between spectral bands is however possible and informative. As discussed in Experimental Methods, some manual alignment of spectra also had to take place for the plan-view samples. Although manual alignment of the energy scale may be necessary between data sets, within one data set the stability of the microscope means that energy shifts within one spectrum image are too small to detect. The C K-edge EELS spectrum (Figure 2b) of the plan-view PA layer shows four characteristic spectral features labelled peak 1 at ~285.1 eV, peak 2 at ~286.4 eV, peak 3 at 288.0 eV, followed by a broad structure 4 above ~289.7 eV. Comparing this energy-loss near-edge fine structure (ELNES) to literature data obtained from XAS experiments, which to a good approximation are extremely similar, allows us to assign the observed peaks to characteristic functional groups[23]. Peak 1 is thus assigned to $1s \rightarrow \pi^*$ transitions, well-known from sp^2-like carbon species.[12,23] XAS studies have, however, shown that a $1s \rightarrow \pi^*$ peak at this energy can arise from carbon or carbonyl groups in an aromatic conformation in PA.[12] Peak 2 can likewise be attributed by comparison to XAS literature to $1s \rightarrow \pi^*$ transitions in nitrated carbon structures[10,20] while Peak 3 at ~288 eV is associated with the carbonyl $1s \rightarrow \pi^*$ C=O transition[12,23] The broad structure 4 above ~289.7 eV can be related to a $1s \rightarrow \sigma^*$ transition.[12] The nitrogen K-edge (at 400 eV) was also acquired under the same experimental conditions and shows three characteristic peaks at ~400 eV, ~401 eV and ~408 eV (Figure 2b). Due to the lower N content, and the well-known challenges with studying functional chemistry at the N K edge, the spectrum is much noisier but is provided here for completeness.[25]

Cross-section across the PA, PSf and resin interface. Figure 2c shows a typical cross section across the PA, PSf and resin. Figure 2d shows EEL spectra taken at the carbon K-edge for the LR white resin and PSf from the cross section samples; an EEL spectrum of the PA membrane from a plan-view sample (as in figure 2b) is plotted on the same figure, for comparison. These spectra have been normalized to the maximum intensity of the $1s$-σ^* region. The large surface area of resin and PSf available - even in a cross-sectional sample - made it possible to acquire these spectra

in identical, dose-managed beam illumination conditions as those used for the PA plan-view spectrum in Figure 2b. The ELNES of the PSf and resin are visibly different to that obtained from the averaged PA spectrum. Here, the first peak is also observed at ~285.1 eV and can similarly be assigned to the $1s \rightarrow \pi^*$ transitions in sp^2-like carbon species, but the next spectral feature for both the PSf and resin appears at around 287.5 eV. This can be assigned by analogy with XAS data to various aliphatic and aromatic carbon species with side chains and/or N-substitutions.[12,26] Although neither the $1s \rightarrow \pi^*$ nor the aliphatic features allow for a robust discrimination between the PSf and the resin, subtle differences in broad spectral features observed at higher energy loss in the $1s \rightarrow \sigma^*$ region (290-305 eV)[26] of the spectrum could be used to discriminate between all three spectra (Figure 2d and Supplementary Information). The effects of beam damage on the shape of fine structure at the C K-edge for the PA, PSf and resin were also tested and are shown in Figure SI1, SI2 and SI3 and described in detail in Supplementary Information.

2. Exploring the effect of the beam on the observed spectral features

A vast number of (likely interdependent) experimental and electron optical parameters influence the effect of the electron beam on samples such as PA thin films. To test whether there exists a set of parameters, and in particular an electron fluence window, compatible with fine structure analysis in spatially resolved EELS spectrum images at the nanometer length-scale, a number of systematic damage experiments were conducted. We systematically recorded spectrum images, whereby a STEM probe (of a given probe size determined by the chosen electron optical setting) is moved serially across a region of interest (or survey area), in a pre-defined number of set positions (number of pixels). At each pixel, both the high-angle annular-dark-field (HAADF) intensity and the EELS signal are recorded over a given duration (or pixel dwell time), thus forming a multi-dimensional dataset containing image and spectral intensity as a function of probe position. These experiments were conducted on the plan-view PA layer sample, with a view to determining how the known spectral features (peaks 1-4 described above) vary as a function of acquisition variables: an area of 800 nm x 800 nm of the sample was systematically irradiated, and the total average EEL spectrum (integrating over all the pixels – of which there may be a varying number) was then inspected after normalization for convenient visualization. The variables selected here were dwell time, pixel spacing and probe size, since these can be conveniently varied

to acquire EEL spectrum images with a given signal-to-noise ratio, while monitoring the evolution of spectral features as a function of exposure to the electron beam: these parameters, and the corresponding calculated electron fluences, are provided in Table 1. This section summarizes the findings of this investigation, while a full discussion of the results of the beam damage experiments is given in Supplementary Information.

Table 1 showing how the corresponding electron fluence per probe size and dose per pixel size vary for each of the acquisition times used in Figure 3.

Acquisition time	Fluence per probe size		Fluence per pixel size	
	C/cm^2	$e/Å^2$	C/cm^2	$e/Å^2$
0.02 s	$1.13x10^4$	$7.03x10^6$	2.56	$1.59x10^3$
0.04 s	$2.26x10^4$	$1.41x10^7$	5.13	$3.18x10^3$
0.06 s	$3.40x10^4$	$2.11x10^7$	7.69	$4.78x10^3$
0.08 s	$4.53x10^4$	$2.81x10^7$	10.3	$6.37x10^3$
0.10 s	$5.66x10^4$	$3.51x10^7$	12.8	$7.96x10^3$
0.12 s	$6.79x10^4$	$4.22x10^7$	15.4	$9.55x10^3$

Acquisition time. The dwell time per pixel was increased from 0.02-0.12 s in increments of 0.02 s (Figure 3a and Figure S1a), at a given large pixel size (5.3 nm). The corresponding electron fluence/probe-size and electron fluence/pixel-size are given in Table 1. Figure 3a shows the evolution of the four characteristic fine-structure features, labelled as peaks 1-4, with increasing fluence. Peaks 1 and 3 decrease in intensity and merge into a broad feature between 284-289 eV. Importantly, peak 2 – which as discussed above can be assigned to C=C-N bonds from the PA membrane using XAS data[12], remains visible above the broadened peak up to an exposure time of 0.12 s, suggesting that this could be used for mapping, even after the other peaks have disappeared due to damage.

11
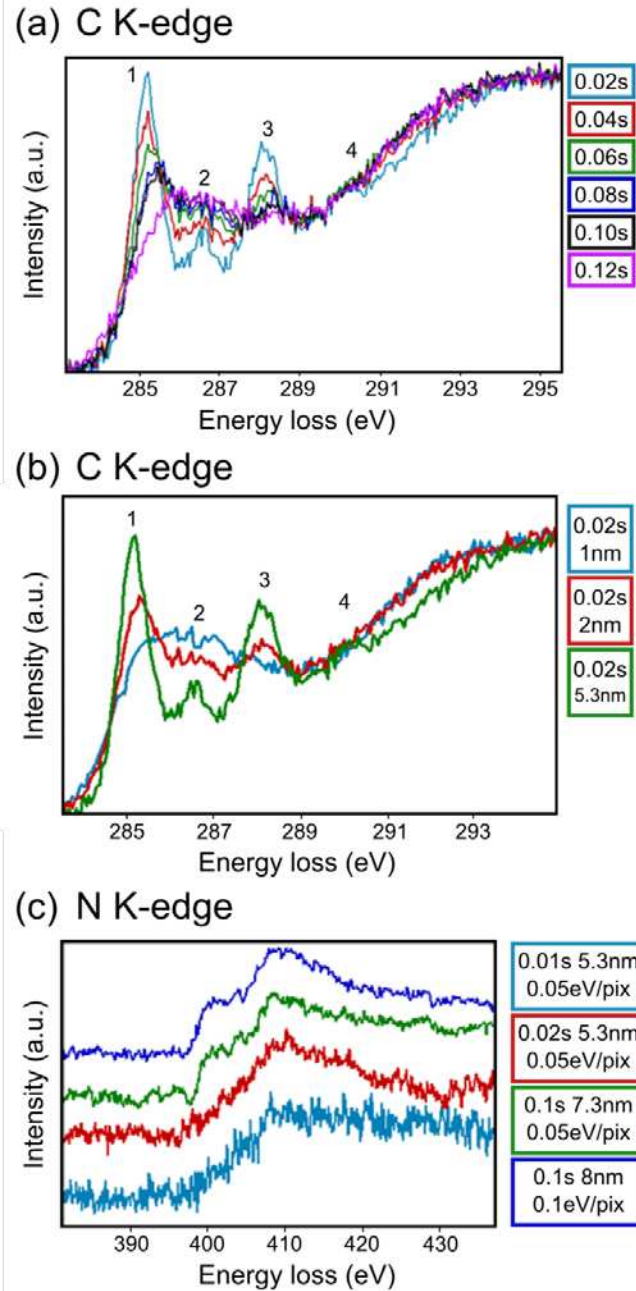
Figure 3 (a) Effect of the acquisition time on the C K-edge fine structure of the plan-view PA film (free standing specimen ~10 nm thick). Spectra were acquired cumulatively for 0.02 s each time on the same region of sample. Dispersion 0.05 eV/pixel, 5.3 nm pixel size, effective energy resolution = 0.2 eV, spectra summed from an 800 x 800 nm area. (b) Effect of pixel spacing on the C K-edge fine structure using a constant acquisition time of 0.02 s. (c) Damage experiments at the N K-edge using different acquisition times and different pixel spacings. Dispersion 0.05 eV/pixel.

Separation between spectra (pixel size). Three-pixel spacings were tested, 1, 2 and 5.2 nm (Figure 3b), using a pixel dwell time of 0.02 s/pixel, which based on the previous discussion, corresponds to the longest acquisition at which no damage was observed in the C K-edge of the PA layer (see Figure S1a). Once more, the intensity of peaks 1-3 is strongly reduced as pixel separation is reduced, with the peaks merging into a broad pre-edge peak at a pixel spacing of 1 nm. Further observations were made for other acquisition times/pixel size combinations (Figure S2). An interesting further consideration is the use of sub-pixel scanning, whereby in some cases (e.g. when the pixel size is larger than the probe size) the probe is continuously rastered within the spatial extent of the pixel while acquiring the EELS signal. Although this strategy can be used to reduce beam damage by avoiding keeping the beam stationary on a single point, it also exposes the entirety of the pixel area to the beam, potentially pre-damaging the next beam position. Given the expected 10 nm width of the PA layers, these pixel-size tests indicate that obtaining any spatially resolved information within the membrane requires using conditions where the EELS fine structure is already modified by the beam.

Probe size. Two different probe sizes, 0.09 nm and 1 nm were tested, corresponding to different electron fluences (See Supporting Information and Figure S1b). Although the larger probe size resulted in a lower electron fluence, the observed influence on the fine structure of the C K-edge is greater. Previous work by Dong *et al.*[17] investigated the effect of probe size on the O K edge fine structure in the EEL spectrum. In this report, both the beam current and the probe size were varied simultaneously, so it was not possible to isolate the effect of probe size alone. A quick calculation using their data suggests that a higher electron fluence was used at larger beam diameters in their case – the opposite to our experimental conditions – and so a clear conclusion about the effect of probe size cannot be inferred from comparing the present work to this earlier study.

For completeness, Figure 3c shows the effect of these parameters on the fine structure of the N K-edge. Due to a much higher noise level characteristic spectral features are only resolved at acquisition times high enough to already cause observable modification of the C K fine structure. The following discussion will therefore focus on an analysis of the C K-edge ELNES, using a 0.09 nm probe and a 0.02 s pixel dwell time, but with a pixel separation of 1nm necessary to resolve spatial changes within the membrane width but which will cause some modification of the observed fine structure.

3. Chemical mapping and spatial localization of a PA membrane using EELS spectrum imaging

Having established the expected fine structure from the various components of the sample, and determined a set of experimental parameters that while knowingly damaging the sample may provide valuable information about the PA separating layer at the nanometer length-scale, it is possible to attempt mapping local chemical variations across the cross-sectioned membrane (Figure 4a-c) using the C, O and N K-edges. The difference in density and average atomic number between the PA membrane, the resin and PSf backing layer leads to differentiable contrast in high-angle annular-dark-field (HAADF) STEM images, whereby the structure identified as the PA membrane exhibits brighter contrast than the surrounding resin (Figure 4a). In this section of the sample, the PSf backing layer seems to have peeled away from the PA membrane itself, so that the membrane has resin on both sides, with the PSf layer visible on the far right-hand side of the HAADF image. Interestingly, judging from the image contrast alone, the edge of the membrane on the left side of the PA appears sharper than on the right side, suggesting some local nanometric "surface roughness". The width of the brighter contrast strip in the images identified as the PA membrane is also wider (around 17 nm if measured from the intensity of the HAADF image) than the expected thickness of the membrane of around 10 nm.[5]

To understand this discrepancy the width of the PA layers was measured from chemical maps generated from a spectrum image (SI) acquired in the area highlighted by a white rectangle in Figure 4a, straddling the resin on the left and right-hand sides of the PA film. As nitrogen is only present in the polyamide and not in the surrounding resin or PSf, it can be used to locate precisely the membrane at the exclusion of all other components. Due to the sample preparation process, a hole in the sample is visible on the right side of the image, which may have resulted in a thickness gradient, the sample thinning down towards the vacuum side. The sample preparation also resulted in the PA and PSf separating and resin infiltrating this region, so that in this particular region of the cross section there is resin on both sides of the separating layer. The chemical maps presented in Figure 4b were obtained by integrating the intensity of the C, N and O ionization edges over a 20 eV energy window, after denoising using principal component analysis (see methods section) and subtraction of the decaying background using a power law. From these maps, average line

profiles were generated demonstrating the relative spatial distribution of these three elements across the mapped region: Figure 4c. As only the PA membrane contains nitrogen, the width of the N map therefore confirms the conclusions drawn from the HAADF image, revealing a ~12 nm wide PA strip, with a sharp edge on the resin side and a rougher edge on the PSf side. The width of the nitrogen-containing region as measured by STEM-EELS SI is in good agreement with the membrane width measured by neutron scattering, as well as with molecular dynamics (MD) simulations[21] previously published by our group for this system (see Figure 1d). These results thus demonstrate that a STEM-EELS N K-edge map can be used to identify unambiguously and arguably more directly than with neutron scattering or MD, the location of a PA membrane in cross-section. Figures 4b and 4c also reveal an unexpected result, the intensity of the O and C profiles is higher around the PA membrane, but are wider than the N-containing region, both with a width of around 17 nm and a higher relative intensity on the top resin-side surface. This suggests some complex functional chemistry and possible reaction between the membrane itself and the surrounding components, which can be further investigated using a more thorough fine structure analysis.
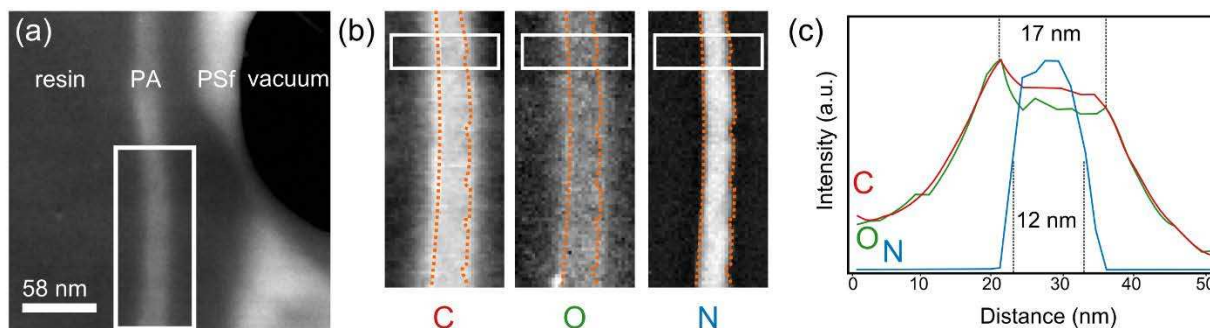

Figure 4 (a) HAADF-STEM image of a PA membrane in cross section. Boxed region (58 nm wide) indicates where the C, O and N elemental maps of the analogue PA membrane in (b) were acquired. The extent of the N signal is highlighted by dotted lines, as a guide to the eyes. (c) Average line profile across the chemical maps in b, using the region highlighted by a white box in (b). The signals were normalised to 1 so that the maps and line profile only reflect the relative spatial content, and not an absolute chemical concentration. The experimental parameters used were: pixel size = 1.7nm, dispersion = 0.3 eV/pixel, effective energy resolution = 0.9 eV, dose per pixel = ~3.7x10^5 e/Å^2. Principal component analysis (PCA) was carried out with 15 factors. Sub-pixel scanning was enabled.

**4. Mapping functional chemistry modulations across the PA active layer at the nanometer length-scale**

The signal-to-noise requirements to obtain spectral fine structure interpretable as representative of specific functional groups make it necessary to use a high electron fluence in spectrum images when attempting to maintain a small probe size and a high sampling rate so as to achieve sub-nm spatial sensitivity. This inevitably leads to experimental conditions under which an organic-based sample such as these PA thin films are expected to suffer significant beam damage, resulting in a loss or an alteration of the observed energy-loss fine structure. Since no other technique can currently provide information at the nm-length-scale, it is nevertheless instructive to test whether interpretable and informative EELS-SI maps can be generated from spectrum images acquired under these conditions. The resulting functional chemistry maps can in turn be correlated with simulated images produced by MD modeling of the PA layer's molecular structure, as a control to establish the extent to which the likely 'damaged' maps retain relevant chemical information.[24]

Figure 5a shows the details of the C K-edge fine structure in spectra taken from two different positions across the PA layer (averaged over pixels to improve signal-to-noise), using the same spectrum image used in Figure 4. This dataset was acquired using an electron fluence of ~3.7×10^5 e/Å^2 per pixel, considerably higher than in the more dose-distributed reference plan-view experiments. Figure 5b reprises the N K-edge map as an indicator of the spatial extent of the PA membrane, although the higher dynamic range display from the colour map used shows that the distribution of N is not homogeneous along the length of the sample of separating layer. The displayed energy range corresponds to the energy window within which the four dominant spectral bands were observed in the plan-view experiments as peaks 1-4 (Figure 3) – which were assigned to known functional groups by analogy with XAS[12]. The visible differences between the spectra in Figure 5a illustrate that despite the likely increased damage due to the higher electron fluence, some spatial variability remains which may be due to changes in the relative contributions of these four spectral features, *albeit* far less pronounced and less straightforwardly interpretable than in the reference experiments.
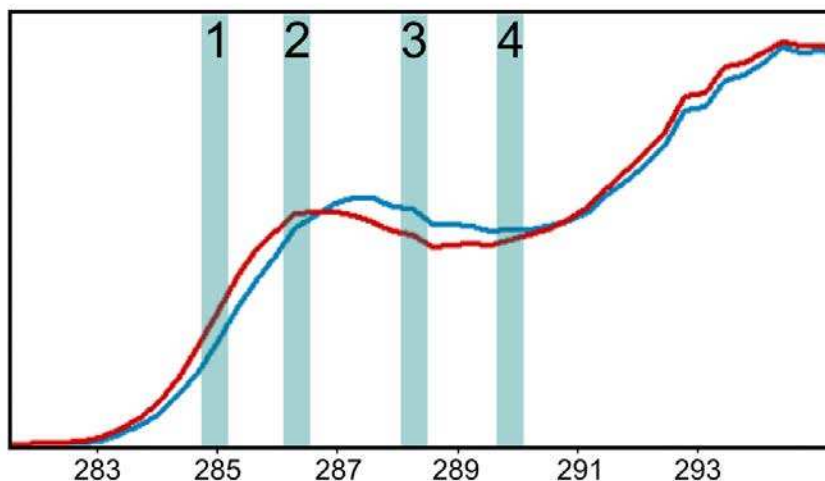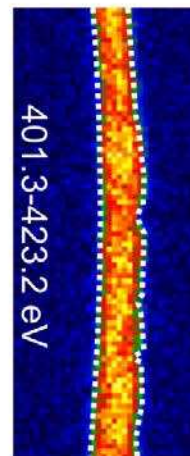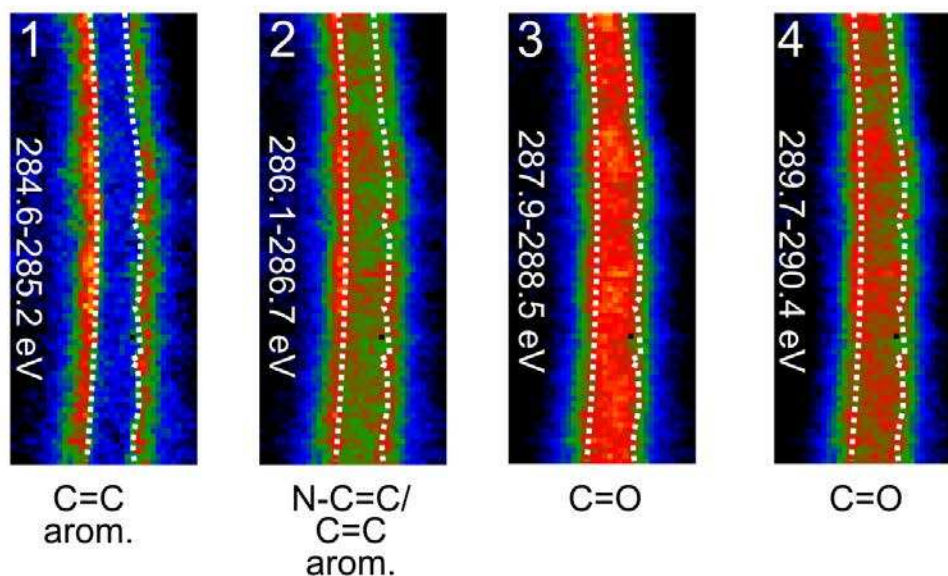
Figure 5 (a) C K-edge spectra from two regions of the spectrum image, demonstrating that fine structure spatial variability remains in spite of likely beam damage. Each of these is summed from a number of adjacent pixels. **(b)** the N K-edge map, as in Figure 4b, is used to identify the extent of the PA membrane. **(c)** False colour maps created by integrating the C K-edge fine structure intensity over energy windows 1-4, corresponding to the 4 spectral bands identified from the plan-view experiments and assigned to specific functional groups using XAS data[12] (Table 2). The experimental parameters used were: pixel size = 1.7nm, dispersion = 0.3 eV/pix, effective energy resolution = 0.9 eV, dose per pixel = ~3.7x10^5 e/Å^2. Principal component analysis (PCA) was carried out with 15 factors. Sub-pixel scanning was enabled.

Integrating the C K-edge intensity over a 0.6 eV wide energy window centered on the energy loss of each of the peaks 1-4 as identified from the plan-view experiments should therefore make it possible to map the relative contribution of the corresponding functional groups across the membrane. The resulting maps (Figure 5c) show that there are significant variations in the spatial distribution of functional groups within the 12 nm layer of the PA membranes. Most intriguing is the strong localization of peak 1 at the very edge of the membrane both on the resin and PSf sides, which XAS studies predict corresponds to a contribution from carbonyl groups. This is also the case, although less marked, for peak 2, corresponding to either aromatic or nitrated functionalities. [12,24] Peaks 2-4, however, also exhibit stronger intensity in regions along the membrane length where the nitrogen signal is also relatively more intense, as seen in Figure 5b.

Machine learning algorithms were employed to gain further insights into the spatial and spectral correlations between these experimental peaks. Non-negative matrix factorization (NMF) in particular (see Materials and Methods section for details on data processing) has been successfully applied to EELS data as an efficient means to unmix signals (or sources of information) contributing to a spectrum image.[27] By enforcing the non-negativity of its output, NMF has the advantage over other machine learning algorithms of producing more straightforwardly interpretable results in terms of spectral factors and their corresponding maps (although as with all machine learning tools, great care must be taken before establishing a direct correspondence between spectral factors and physical signals). Figure 6a illustrates the relative contribution across the mapped area of each of the first 6 factors derived from the NMF analysis. These factors, labeled A-F, are in turn plotted in Figure 6b for the entire energy range recorded in the spectrum image (250-600 eV), while the details over the carbon K-edge energy range (283-295 eV), where peaks 1-4 were identified earlier, are presented in Figure 6c.
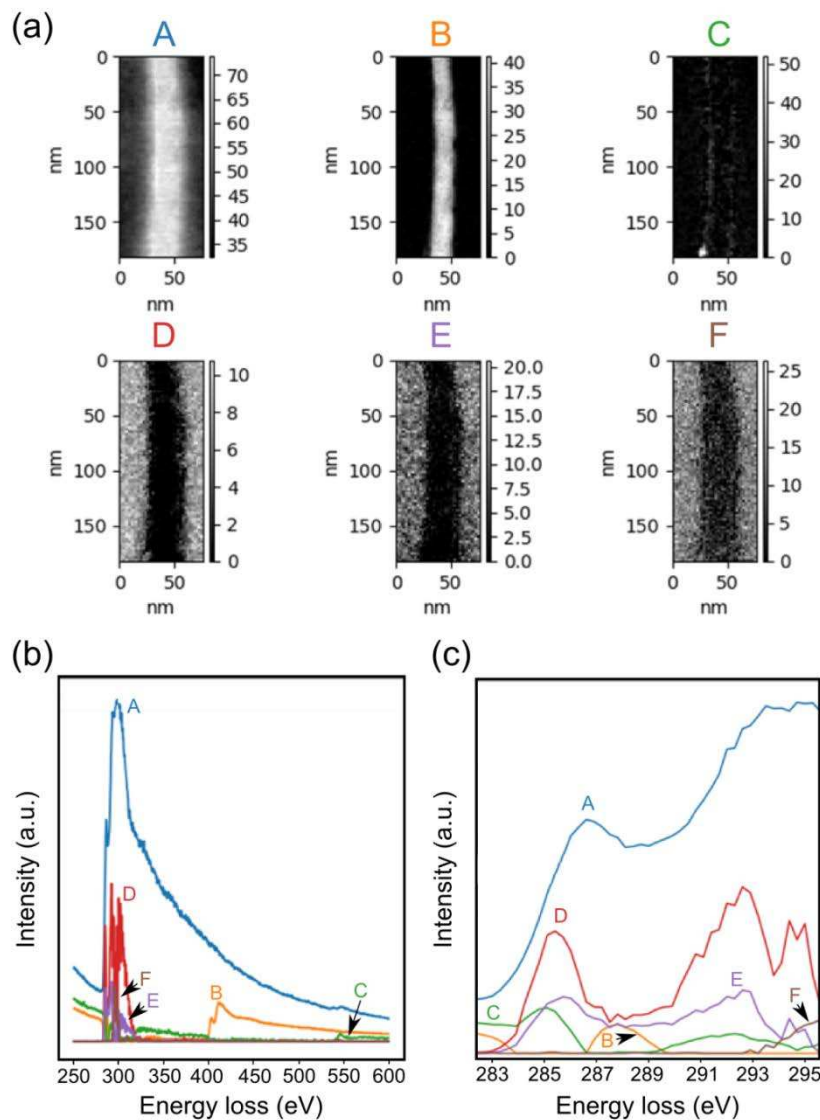
Figure 6 Non-negative matrix factorisation (NMF) of analogue PA membrane from Figure 4. The data set was first denoised by principal component analysis (PCA) and 15 components were used for subsequent NMF analysis. (a) Visual representation of the SI reconstructed from the first 6 NMF components A-F; (b) Representation of factors A-F covering the full spectral range, including the C, N and O K-edges; (c) A high magnification region of the spectral range in (b) covering energy range of 1s→π* region of C K-edge. Component B shows strong localisation throughout the central region of the membrane, and elicits a strong peak at the N K-edge (b) and an associated peak at 287.8 eV in the C K-edge, which is absent from the other components. This component can be confidently assigned as arising from transitions to N-C=C bonds within the membrane, as it matches well (within 0.1 eV) the known energy of the spectral signature of this functional group derived from XAS data.[12]

19

Three of the factor maps (D-F) exhibit a strong localization only outside of the membrane area, with no intensity in the energy range corresponding to the N or O K ionization edges This localization is clear, even though their contribution to the overall signal was weak (as seen in the spectral representation in Fig 6b), suggesting that these maps are representative of the specific functional chemistry of the resin and/or PSf backing layer A more detailed analysis of their spectral weights in the C K energy range, Figure 6c, reveals the existence of distinct contributions to the C K-edge of the resin and PSf, with peak maxima at 285.5, 292.8 and 295 eV (factors D and E), and a sloping contribution from 295eV onwards (factor F). The relatively lower spectral weight in the 286-291eV range, with stronger contributions in the π^* and σ^* region of the edge provides a good match with the experimental reference spectra in Figure 2 and confirms the identification of these factors as being associated with the resin.

Factor C exhibits a strong spectral weight at the O K edge (535 eV) and is highly localized to a single region of the spectrum image (the bright spot at the bottom left of the corresponding map in Figure 6b), suggesting it relates mostly to a local impurity, also evident in the O K map in Figure 4. Some additional localization of factor C along the edges of the PA membrane is consistent with the presence of O outside of the N-containing membrane. Most interesting is factor B, which exhibits a distinctly strong peak at the N K-edge (~400 eV, Figure 6b) and an associated peak at ~287.6 eV in the C K-edge. This peak, which is absent from the other factors, would constitute a good match for peak 2 in our reference data, which XAS data suggests corresponds to transitions in nitrated carbon structures, and in particular N-C=C bonds[12,24]. The map constructed using factor B also shows strong localisation throughout the central region of the membrane only, with the same intensity fluctuation through its length as observed in the N K map (comparing Figure 5b and Figure 6a). We therefore suggest that factor B may be assigned as arising from transitions to N-C=C bonds within the membrane, whose spatial localization would then appear to vary along the length of the membrane (which may be intrinsic to the material but also possibly due to a variety of reasons, including possible beam damage or sample preparation artefacts).

Factor A, which has the most dominant contribution to the PA membrane, correlates to the regions that are carbon-rich but lacking strong functional chemistry. The corresponding representation of the C K-edge spectral range in Fig 6b reveals a 1s→π^* peak shape expected of a 'generic' amorphous carbon signal. The representation of factor A in Fig 6a corresponds well to the 'generic' C K-edge signal observed from experimental data in Fig 4b, also suggesting that this is

mostly generated from a generic amorphous C signal. Additionally, there is a contribution from oxygen to in factor A (at 535 eV) which agrees with experimental data showing that a small amount of O is present in the membrane and at the membrane surfaces (Fig 4b). The more dominant contribution from oxygen is found in Factor C which, as discussed above, is primarily localized to the surface of the membrane.Table 2 summarizes this analysis and the spectral band assignments that were made possible by comparing experimental data, both dose managed and at high doses, a machine learning (NMF) decomposition into spectral contributions, and known spectral band assignments from XAS results in the literature.

Table 2 Principal C K-edge peak positions used to map chemical functionality across the PA membrane and comparison with X-ray spectroscopy and NMF processing

	Peak position from Figure 2b (eV)	Peak positions from ref. XAS data [10] (eV)	Peak Assignment from ref. [10]	Maxima in components of NMF, applied to data set in Figure 6 (eV)
1	285.1	284.9-285.2	$1s \rightarrow \pi^*$(C=C aromatic)	285.0
2	286.4	286.4-286.9	$1s \rightarrow \pi^*$(N-C=C) $1s \rightarrow \pi^*$(C=C)	286.7
3	288.0	287.8-289.0	$1s \rightarrow \pi^*$(C=O carbonyl)	**287.8 (Component B that includes a strong N K-edge peak)**

5. Application to commercial RO membranes

Finally, it is instructive and industrially relevant to attempt to apply the same methodology to cross-sectioned SW30HR (Dow Chemical Company, USA) sheet membranes. Here the well-known complex crumpled "ridge and valley" morphology, makes the analysis particularly challenging compared to the idealized flat PA separating layers used above. HAADF-STEM

images of these membranes illustrate this complexity, with folds and protuberances (Figure 7a) and "channels" (thin regions of dark contrast observed between walls of material with brighter contrast: Figure 7b). Chemical maps using the N K-edge, which was established as a reliable means of localizing the PA separating layer, revealed individual N-rich structures of approximate 10 nm width, which we interpret as folded membrane sheets forming a hollow region between the folds[9]. The presence of "channels" has previously been observed by our group, through exposing these membranes to a RuO_2 vapour stain.[4] Here, using the EELS-SI technique, we are able to confirm that the folded and crumpled sheet like structures are internally hollow and can be imagined by considering "deflated balloons" rather than solid nodules or tongues. This is of high importance, since it re-inforces our assertion that it is the crumpled nature of the PA separating layer that increases its surface area and results in the permeance of a commercial membrane being 2 x 4 times higher than the permeance of an analogue thin film which is made completely smooth. Rather than solid shapes, the separating layer of a commercial TFC RO membrane can be imagined as a thin film, or the order 10 nm in thickness that folds and re-folds on itself during the interfacial polymerization process, so that each square meter of membrane support has between 2 and 4 m^2 of membrane separating layer.
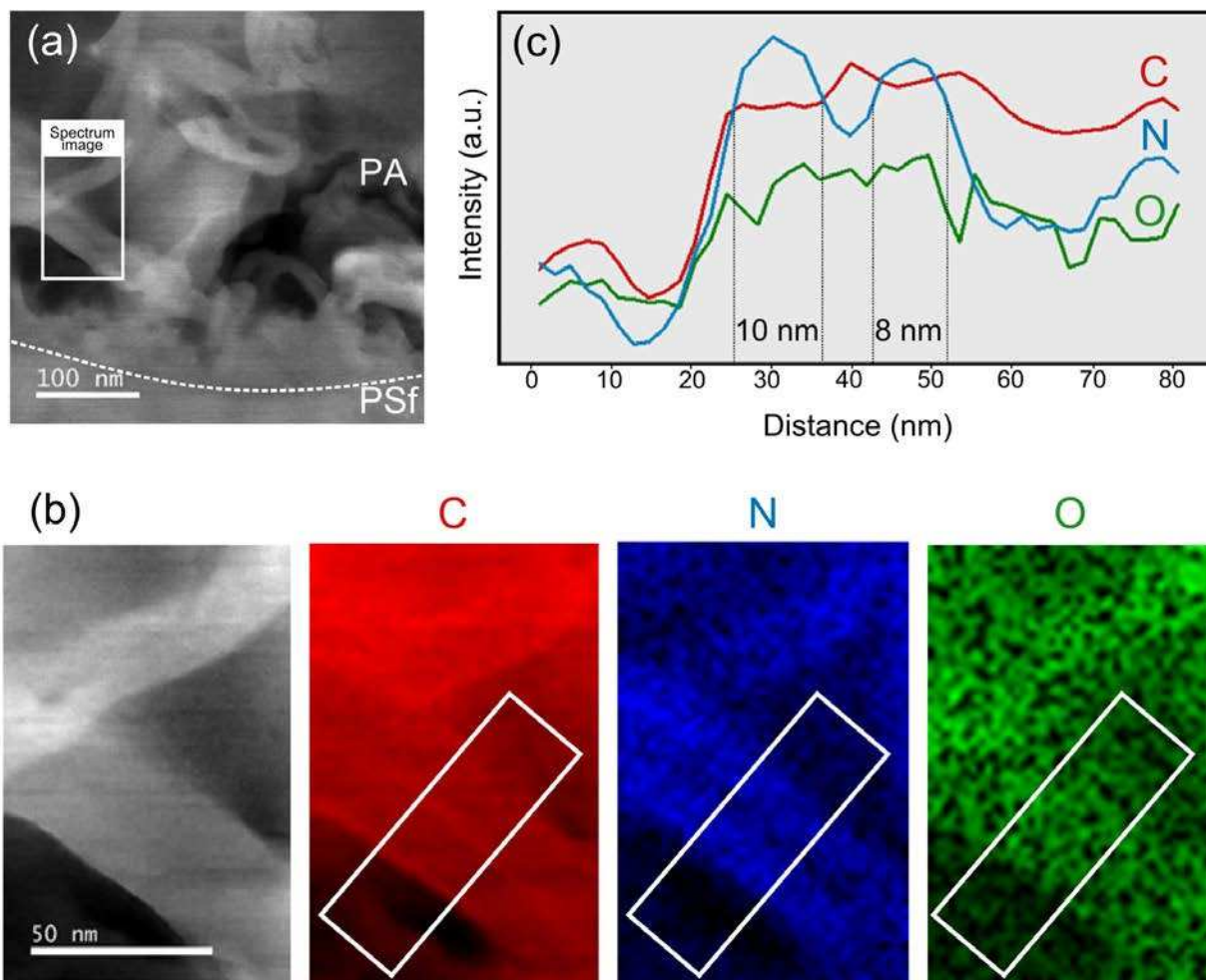
Figure 7. Elemental mapping of SW30HR DOW membrane. (a) Protuberances of the PA layer formed on the PSf support. b) Elemental maps of carbon, nitrogen and oxygen K-edges from the region highlighted in (b). (c) Intensity profiles across the maps in (b) showing separation and thickness of the PA film.

CONCLUSIONS

The development of a thin and flat membrane by Karan *et al.*[11] has provided the opportunity to attempt to map the functional chemistry within thin PA membranes without the extra challenges involved in studying complex commercial samples.[4,10] We were able to show that the location of the PA film of both flat, in-house fabricated, 10 nm thick PA films and rough, commercially available membranes can be determined using EELS-SI chemical mapping at the N K-edge. By combining information from careful beam damage experiments, reference data (either EELS-based, dose managed data with no spatial resolution, or literature XAS or neutron scattering

23

results), it was possible to map nano-scale chemical variations within the PA layer attributed to variations in the distribution of N-C=C bonds. This was achieved taking the pragmatic approach that although spatial localization necessarily implied a degree of alteration in the observed spectral fine structure, these "damaged" data sets can still be used to infer useful information that cannot be obtained with any other experimental technique. We note that the PA sample studied here appeared to have a much higher damage threshold compared to many polymers studied in the literature[28] and the use of newer detectors may, in future, allow polymers with a much lower threshold to be studied – firstly to identify the peaks in the undamaged data and subsequently to study damaged spectra with high spatial resolution. Current technological developments in the field of electron microscopy, such as stable cold sample stages, and high frame-rate cameras with direct electron detection capabilities will in the near future make it possible to further refine the experimental parameters required for high spatial and energy resolution studies of soft materials.[29] The nanoscale chemical pathways that can be deduced from this analysis show that the active PA layer of the RO membranes is highly heterogeneous at the nanoscale, which offers a clearer understanding of the transport mechanisms through the membrane.

MATERIALS & METHODS

Sample preparation

The ultrathin film polyamide (PA) films used for the majority of this study were fabricated by the interfacial polymerization of MPD and TMC at the water/hexane interface onto a sacrificial $Cd(OH)_2$ nanostrand layer supported by an ultrafiltration polysulfone membrane, following the procedure reported by Karan *et al.*[11] TMC (98%) and MPD flakes (99+%) were purchased from Sigma-Aldrich and spectroscopic grade solvents (VWR International) and deionized water (Millipore) were employed. The $Cd(OH)_2$ nanostrand/polysulfone layer was first soaked in 25 mL aqueous solutions of 0.1 wt% MPD; film formation was then initiated by carefully pouring 25 mL of the TMC/hexane at 0.005 wt% solution. The reaction was allowed to proceed for 10 min, following the removal of unreacted TMC with excess hexane, and finally removal of the sacrificial nanostrand layer by dissolution in acidified water. The resulting PA membrane was then transferred onto a polysulfone (PSf) support film.

The cross-sectional profile and film thickness was measured by specular neutron reflectivity at the D17 reflectometer of the Institut Laue Langevin (ILL, Grenoble, France) at angles 0.5 and 3.0, covering a momentum transfer normal to the surface ($q_z = (4\pi/\lambda)\sin\theta$) ranging from 0.006 to 0.3 Å^{-1}. Data were analyzed employing the RasCAL software. Similar thickness measurements were obtained by atomic force microscopy.

Plan view TEM samples were prepared by removing the polyester backing layer and dissolving the PSf layer in dimethyl fluoride (DMF) leaving the PA layer floating on top of the solution. The PA was then picked up on a holey carbon TEM grid. This follows a similar procedure to the schematic outlined by Karan *et al.* in SI Fig. S14[9]. In our case the hydrochloric acid (HCl) was replaced with DMF and a holey-C film was used instead of a Si wafer. The grid was then washed several times in water to remove any residual DMF.

Cross-section TEM samples of the PA and PSf layers were prepared by peeling off the polyester backing layer and embedding the remaining PA and PSf layers in LR white resin following the protocol in reference[4]. LR white resin was used as it helps to enhance contrast between the membrane and resin.[30] Thin sections were cut with a diamond knife in a PowerTome Ultramicrotome (Boeckeler Instruments, Tucson, USA) and collected onto plain TEM Cu grids or holey carbon support films.

Electron energy-loss spectroscopy (EELS)

High energy resolution electron energy-loss spectroscopy (EELS) experiments were carried out at SuperSTEM (Daresbury, UK) on the Nion UltraSTEM 100MC 'HERMES' monochromated electron microscope. The microscope was operated at 100 kV with a scanning transmission electron microscopy (STEM) probe size of 0.9 Å at a convergence semi-angle of 31 mrad. The monochromator slit was adjusted to deliver an energy resolution of 0.15eV, as estimated from the full-width at half-maximum (FWHM) of the zero-loss (ZL) peak when the monochromator slit was inserted. EELS spectra were recorded on a Gatan Enfinium ERS spectrometer with a collection semi-angle and 44 mrad. Probe currents between 7 and 150 pA were used depending on the required energy resolution and opening of the monochromator slit. All spectra were acquired with 130x vertical binning. Observations of these systems in cryo-conditions, which may help to

reduce the effect of beam damage[31-32], should be possible in the future thanks to new stage designs currently being prototyped[33].

The electron fluence (electron/Angstrom^2) and electron flux (electron/Angstrom^2/second) values at each point are given in each figure or figure caption. Two methods can be used to calculate the electron flux: one is the electron flux per probe size (e.g. the flux in a circular 0.9Å probe), the other is the electron flux per pixel which assumes the flux is spread across the square pixel. Table 2 gives a comparison of these two methods for one data set. The value given for beam damage experiments is per probe size and those for the cross-section samples are per pixel size due to sub-pixel scanning having been used. A discussion of the advantages of each method can be found in the supporting information.

Cross-Section samples:

For EELS experiments on the cross-section samples, long, straight regions of the membrane were chosen. The experimental parameters used were: pixel size of 1.7 nm, dispersion of 0.3 eV/pix, effective energy resolution of 0.9 eV and a fluence per pixel of $3.7x10^5$ e/Å^2. Sub-pixel scanning was used, and so the electron dose calculation was based on pixel size.

Data sets were aligned using the maximum of the zero-loss peak. Where necessary, data sets can be re-aligned within each spectrum image (SI) to account for unwanted jitters or energy drifts. However, due to the use of advanced energy stabilization schemes,[34] and the relatively small dispersions used for this work, this was not usually required.

Principal Component Analysis (PCA) as implemented in Hyperspy[35] was used in order to improve the signal-to-noise ratio (SNR). The individual components were checked to make sure no significant data was removed. Typically, 15 components were chosen. No other processing was done on the data to avoid the introduction of artefacts.

EELS-SI elemental maps were constructed by integrating across suitable energy windows at the C, N and O K-edges. EELS–SI maps showing fine structure within the C K-edge were constructed in a similar way using narrower energy windows, around 0.6 eV wide. The same data sets were used to obtain the elemental maps and the fine structure maps.

Beam damage experiments on plan-view samples

Flat, free-standing regions of the plan-view ~10 nm thick analogue separating layer were used for beam damage experiments. EELS-SIs were acquired over arrays of pixels (e.g. 100x100 pixels or 150x150 pixels) using low dwell times per pixel (as indicated in the captions of each figure). The spectra acquired from the whole region were summed to improve the signal-to-noise ratio (SNR). Sub-pixel scanning was not used for these experiments unless otherwise stated. A fluence per probe size was calculated.

Once the experimental conditions had been set, new regions of the PA layer which had not been previously exposed to the beam were moved into the "field of view" with the beam blanked. After this 1-2 minutes were given for the stage to settle before starting the acquisition. For spectral acquisition, the beam remained blank for the first few pixels of the SI and only unblanked once the SI had fully started to avoid overexposure of the sample to the beam. These pixels were ignored when summing the data.

For some of the beam damage experiments the zero-loss region was not acquired simultaneously with the core-loss region to reduce the total exposure to the electron beam. As a result, in some cases (Figure 5 and Figures SI1-2,4) manual alignment of the spectra was required. In these cases peak 1 in the least damaged spectrum was aligned to 285.1 eV in agreement with data from X-ray spectroscopy.[12]

More details of the beam damage experimental set up can be found in the Supplementary Information.

Processing algorithms and procedures

Non-negative matrix factorization (NMF), a machine learning algorithm shown to be very effective in processing EELS data, was employed to carry out further numerical analysis on spectrum images of the analogue PA separating layer. NMF is typically applied after an initial principal component analysis (PCA) step, to denoise the data and remove non-statistically significant sources of information within.[36] All machine learning analysis steps were carried out using the HyperSpy package.[35]

NMF has the advantage over other similar algorithms that imposes that all the factors be non-negative, which can aid interpretation as the spectral shape of the resulting components is often closer to the spectroscopic signature of relevant bonding-related signals. A large number of iterations were typically carried out (~80). The first few components in the decomposition were the most significant in contributing to the model spectra, both in terms of their spatial localisation (clearly relating to the geometry of the area investigated) and of their respective spectral shape (components of index 7 or above visually appeared to correspond to noise rather than to significant spectral information). The relevant components were plotted both spatially as localisation maps, and as factors which resemble spectra (although care must be taken to interpret these directly as physically-meaningful spectral information). The images created from the factors' spatial localisation, and the spectral weight the factors themselves, provides instructive comparisons to reference data.

ASSOCIATED CONTENT

Supporting Information. A listing of the contents of each file supplied as Supporting

Information is included.

AUTHOR INFORMATION

Corresponding Author

*To whom all correspondence should be addressed:

*Prof. Alexandra Porter and Dr. Catriona McGilvery, Imperial College London, Department of

Materials, Royal School of Mines, London SW7 2AZ, UK. Tel: +44 (0) 20 7594 9691, email:

a.porter@imperial.ac.uk and catriona.mcgilvery@imperial.ac.uk

Present Addresses

†Patricia Abellan, Institut des Matériaux Jean Rouxel, CNRS, France, email.

Patricia.Abellan@cnrs-imn.fr

Author Contributions

P.A, C.M.M. and Q.R. carried out the majority of experiments. P.A, C.M.M. and Q.R. conducted the SuperSTEM EELS experiments. C.M.M. and M.K. conducted the TEM work at Imperial College. M.K. prepared the TEM specimens. All authors designed the project and analyzed the data. A.E.P., C.M.M. and Q.R wrote the paper with through contributions of all authors. All authors have given approval to the final version of the manuscript.

REFERENCES

(1)   Pinnau, I.; Freeman, B. D. Formation and Modification of Polymeric Membranes: Overview. *In Membrane Formation and Modification*; A*CS Symposium Series; American Chemical Society,* 1999; *744*, 1–22.

(2)   Freger, V. Nanoscale Heterogeneity of Polyamide Membranes Formed by Interfacial Polymerization. *Langmuir* 2003, *19* (11), 4791–4797.

(3)   Coronell, O.; Mariñas, B. J.; Cahill, D. G. Depth Heterogeneity of Fully Aromatic Polyamide Active Layers in Reverse Osmosis and Nanofiltration Membranes. *Environ. Sci. Technol.* 2011, *45* (10), 4513–4520.

(4)   Kłosowski, M. M.; McGilvery, C. M.; Li, Y.; Abellan, P.; Ramasse, Q.; Cabral, J. T.; Livingston, A. G.; Porter, A. E. Micro-to Nano-Scale Characterisation of Polyamide Structures of the SW30HR RO Membrane Using Advanced Electron Microscopy and Stain Tracers. *Journal of Membrane Science* 2016, *520*, 465–476.

(5)   Foglia, F.; Karan, S.; Nania, M.; Jiang, Z.; Porter, A. E.; Barker, R.; Livingston, A. G.; Cabral, J. T. Neutron Reflectivity and Performance of Polyamide Nanofilms for Water Desalination. *Advanced Functional Materials* 2017, *27* (37), 1701738.

(6)   Hughes, Z.E.; Gale, J.D. A computational investigation of the properties of a reverse osmosis membrane. *J. Mater. Chem.* 2010, *20*(36):7788–7799.

(7)   Kolev, V.; Freger, V. Hydration, porosity and water dynamics in the polyamide layer of reverse osmosis membranes: A molecular dynamics study. *Polymer* 2014, 55(6). 1420 – 1426.

(8)   Coronell, O.; Mariñas, B. J.; Zhang, X.; Cahill, D. G. Quantification of Functional Groups and Modeling of Their Ionization Behavior in the Active Layer of FT30 Reverse Osmosis Membrane. *Environ. Sci. Technol.* 2008, *42* (14), 5260–5266.

(9)   Tang, C. Y.; Kwon, Y.-N.; Leckie, J. O. Effect of Membrane Chemistry and Coating Layer on Physiochemical Properties of Thin Film Composite Polyamide RO and NF Membranes: II. Membrane Physiochemical Properties and Their Dependence on Polyamide and Coating Layers. *Desalination* 2009, *242* (1–3), 168–182.

(10)   Li, Y.; Kłosowski, M. M.; McGilvery, C. M.; Porter, A. E.; Livingston, A. G.; Cabral, J. T. Probing Flow Activity in Polyamide Layer of Reverse Osmosis Membrane with Nanoparticle Tracers. *Journal of Membrane Science* 2017, *534*, 9–17.

(11)   Karan, S.; Jiang, Z.; Livingston, A. G. Sub–10 Nm Polyamide Nanofilms with Ultrafast Solvent Transport for Molecular Separation. *Science* 2015, *348* (6241), 1347–1351.

(12)   Mitchell, G. E.; Mickols, B.; Hernandez-Cruz, D.; Hitchcock, A. Unexpected New Phase Detected in FT30 Type Reverse Osmosis Membranes Using Scanning Transmission X-Ray Microscopy. *Polymer* 2011, *52* (18), 3956–3962

(13)   Kaznatcheev, K. V.; Karunakaran, Ch.; Lanke, U. D.; Urquhart, S. G.; Obst, M.; Hitchcock, A. P. Soft X-Ray Spectromicroscopy Beamline at the CLS: Commissioning Results. *Nuclear Instruments and Methods in Physics Research Section A: Accelerators, Spectrometers, Detectors and Associated Equipment* 2007, *582* (1), 96–99.

(14)   Goode, A. E.; Porter, A. E.; Ryan, M. P.; McComb, D. W. Correlative Electron and X-Ray Microscopy: Probing Chemistry and Bonding with High Spatial Resolution. *Nanoscale* 2015, *7* (5), 1534–1548.

(15)   Krivanek, O. L.; Lovejoy, T. C.; Dellby, N.; Carpenter, R. W. Monochromated STEM with a 30 MeV-Wide, Atom-Sized Electron Probe. *Microscopy (Oxf)* 2013, *62* (1), 3–21.

(16) Krivanek, O. L.; Lovejoy, T. C.; Dellby, N.; Aoki, T.; Carpenter, R. W.; Rez, P.; Soignard, E.; Zhu, J.; Batson, P. E.; Lagos, M. J.; Egerton, R. F.; Crozier, P.A. Vibrational Spectroscopy in the Electron Microscope. *Nature* 2014, *514* (7521), 209–212.

(17) Dong, W.; Hakukawa, H.; Yamahira, N.; Li, Y.; Horiuchi, S. Mechanism of Reactive Compatibilization of PLLA/PVDF Blends Investigated by Scanning Transmission Electron Microscopy with Energy-Dispersive X-ray Spectrometry and Electron Energy Loss Spectroscopy. *Applied Polymer Materials* 2019, *1,* 815-824

(18) Egerton, R. F. Radiation Damage to Organic and Inorganic Specimens in the TEM. *Micron* 2019, *119*, 72–87.

(19) S'ari, M.; Blade, H.; Brydson, R.; Cosgrove, S. D.; Hondow, N.; Hughes, L. P.; Brown, A. Toward Developing a Predictive Approach To Assess Electron Beam Instability during Transmission Electron Microscopy of Drug Molecules. *Mol. Pharmaceutics* 2018, *15* (11), 5114–5123.

(20) Egerton, R. F.; Lazar, S.; Libera, M. Delocalized Radiation Damage in Polymers. *Micron* 2012, *43* (1), 2–7.

(21) Muscatello, J.; Müller, E. A.; Mostofi, A. A.; Sutton, A. P. Multiscale Molecular Simulations of the Formation and Structure of Polyamide Membranes Created by Interfacial Polymerization. *Journal of Membrane Science* 2017, *527*, 180–190.

(22) Egerton, R.F. Control of Radiation Damage in the TEM *Ultramicroscopy* 2013, *127*, 100-108

(23) Hitchcock, A.P.; Dynes, J.J.; Johansson, G.; Wang, J.; Botton, G. Comparison of NEXAFS microscopy and TEM-EELS for studies of soft matter, *Micron*, 2008, 39, 741–748

(24) Urquhart, S. G.; Ade, H. Trends in the Carbonyl Core (C 1S, O 1S) → Π* $_{C=O}$ Transition in the Near-Edge X-Ray Absorption Fine Structure Spectra of Organic Molecules. *The Journal of Physical Chemistry B* 2002, *106* (34), 8531–8538.

(25) Vollmer, C.; Leitner, J.; Kepaptsoglou, D.; Ramasse, Q.M.; Busemann, H.; and Peter Hoppe. Isotopic compositions, nitrogen functional chemistry, and low-loss electron spectroscopy of complex organic aggregates at the nanometer scale in the carbonaceous carbonaceous chondrite Renazzo. *Meteoritics & Planetary Science* 2019, 1–27.

(26) Lehmann, J.; Solomon, D.; Brandes, J.; Fleckenstein, H.; Jacobson, C.; Thieme, J. Synchrotron-Based Near-Edge X-Ray Spectroscopy of Natural Organic Matter in Soils and Sediments. In *Biophysico-Chemical Processes Involving Natural Nonliving Organic Matter in Environmental Systems*; John Wiley & Sons, Ltd, 2009; pp 729–781.

(27) Collins, S.M.; Ringe, E.; Duchamp, M.; Saghi, Z.; Dunin-Borkowski, R.E.; and Midgley, P.A. Eigenmode Tomography of Surface Charge Oscillations of Plasmonic Nanoparticles by Electron Energy Loss Spectroscopy. *ACS Photonics*, 2015, 2, 1628-1635.

(28) Wang, J., G.A. Botton, M.M. West, and A.P. Hitchcock, Quantitative Evaluation of Radiation Damage to Polyethylene Terephthalate by Soft X-rays and High-energy Electrons. *The Journal of Physical Chemistry B* 2009, 113, 1869-1876.

(29) Alexander, J. A.; Scheltens, F. J.; Drummy, L. F.; Durstock, M. F.; Hage, F. S.; Ramasse, Q. M.; McComb, D. W. High-Resolution Monochromated Electron Energy-Loss Spectroscopy of Organic Photovoltaic Materials. *Ultramicroscopy* 2017, *180*, 125–132.

(30) Pacheco, F. A.; Pinnau, I.; Reinhard, M.; Leckie, J. O. Characterization of Isolated Polyamide Thin Films of RO and NF Membranes Using Novel TEM Techniques. *Journal of Membrane Science* 2010, *358* (1), 51–59.

(31)   Dubochet, J., Adrian, M., Chang, J. J., Homo, J. C., Lepault, J., McDowall, A. W., Schultz, P. Cryo-Electron Microscopy of Vitrified Specimens. *Quarterly reviews of biophysics*, 1998 *21* (2), 129-228.

(32)   Ilett, M., Brydson, R, Brown, A., Hondow, N., Cryo-Analytical STEM of Frozen, Aqueous Dispersions of Nanoparticles, *Micron* 2019, *120*, 35-42

(33)   Hotz, M.T., Corbin, G., Dellby, N., Lovejoy, T.C., Skone, G.S., Blazit, J.D., Kociak, M., Stephan, O., Tence, M., Zandbergen, H.W., Krivanek, O. L., Optimizing the Nion STEM for in-situ Experiments, *Microscopy & Microanalysis* 2018 *24* (Suppl. 1), 1132-1133

(34)   Krivanek, O. L.; Ursin, J. P.; Bacon, N. J.; Corbin, G. J.; Dellby, N.; Hrncirik, P.; Murfitt, M. F.; Own, C. S.; Szilagyi, Z. S. High-Energy-Resolution Monochromator for Aberration-Corrected Scanning Transmission Electron Microscopy/Electron Energy-Loss Spectroscopy. *Philosophical Transactions: Mathematical, Physical and Engineering Sciences* 2009, *367* (1903), 3683–3697.

(35)   *Hyperspy: Hyperspectral Data Analysis Toolbox*; 2013.

(36)   Collins, S. M.; Ringe, E.; Duchamp, M.; Saghi, Z.; Dunin-Borkowski, R. E.; Midgley, P. A. Eigenmode Tomography of Surface Charge Oscillations of Plasmonic Nanoparticles by Electron Energy Loss Spectroscopy. *ACS Photonics* 2015, *2* (11), 1628–1635.

Cover Art
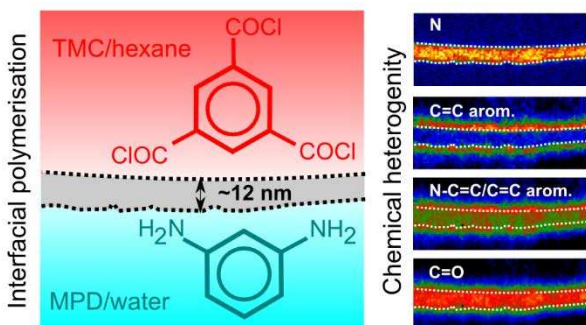
The nanoscale distribution of functional chemistry across 12 nm thick polyamide reverse osmosis membranes, prepared via interfacial polymerisation, has been mapped using scanning transmission electron microscopy electron energy-loss spectroscopy. Chemical maps show nanometer scale variations in chemical heterogeneity within the membranes that may play a role in solute filtration.